Multistable Cosine-Curved Dome System for Elastic Energy Dissipation

Mansour Alturki
Department of Civil and Environmental Engineering,
Michigan State University,
1208 Engineering Building,
East Lansing, MI 48824-1226
e-mail: alturki1@msu.edu

Rigoberto Burgueño[1]
Professor
Department of Civil and Environmental Engineering,
Department of Mechanical Engineering,
Michigan State University,
3574 Engineering Building,
East Lansing, MI 48824-1226
e-mail: burgueno@msu.edu

This paper presents a new energy dissipation system composed of multistable cosine-curved domes (CCD) connected in series. The system exhibits multiple consecutive snap-through and snap-back buckling behavior with a hysteretic response. The response of the CCDs is within the elastic regime and hence the system's original configuration is fully recoverable. Numerical studies and experimental tests were conducted on the geometric properties of the individual CCD units and their number in the system to examine the force–displacement and energy dissipation characteristics. Finite element analysis (FEA) was performed to simulate the response of the system to develop a multilinear analytical model for the hysteretic response that considers the nonlinear behavior of the system. The model was used to study the energy dissipation characteristics of the system. Experimental tests on 3D printed specimens were conducted to analyze the system and validate numerical results. Results show that the energy dissipation mainly depends on the number and the apex height-to-thickness ratio of the CCD units. The developed multilinear analytical model yields conservative yet accurate values for the dissipated energy of the system. The proposed system offered reliable high energy dissipation with a maximum loss factor value of 0.14 for a monostable (self-recoverable) system and higher for a bistable system.
[DOI: 10.1115/1.4043792]

1 Introduction

Increased attention has been recently given to systems that utilize elastic instabilities for energy dissipation and shock absorption [1]. The reason is that the mechanical deformations of such systems are fully reversible since the total response is within the elastic regime of the constituent base material [2]. Usually, these systems consist of parallel chains of multistable elements or unit cells that are connected in series and respond to a common load in a progressive manner. When these elements are loaded under displacement control conditions, they show negative stiffness region due to geometric nonlinearity [3]. The consecutive snap-through buckling events of the repeating units enable attaining a hysteretic force–deformation response. These systems can thus be used to elastically absorb and dissipate energy. Most of these structures rely on two basic types of multistable elements. The first type includes inclined beams or bars [4–7], where the member is transversely loaded at one end through its projection causing it to snap-through while the other end is fixed. The second type includes curved beams or bars [8–15] that are transversely loaded at their apex and fixed at both ends.

A new energy dissipation system comprising multiple cosine-curved domes (MCCD) connected in series is presented herein. The building units of the MCCD system are dome-shaped shell elements called cosine-curved domes (CCD) studied by the authors in an earlier work [16], see Fig. 1(*a*). The noted former study introduced the multistable element (CCD), showed how it can attain a controllable snap-through instability, and presented its response characteristics, with the motivation of using it in a system for elastic energy dissipation. A CCD can exhibit snap-through buckling behavior in monostable and bistable states as shown in Fig. 1(*b*). When an MCCD system (see Fig. 1(*c*)) is mechanically loaded, the CCD units consecutively snap-through to a new stability state within their elastic range. When the system is unloaded, the units consecutively snap-back to their original configuration, either by a restoring external force for bistable CCDs or by self-recoverability (preferred) for monostable CCD units. If a sufficient number of connected units in series is used, the MCCD system follows distinct loading and unloading paths resulting in a hysteretic response, as shown in Fig. 1(*d*). The area enclosed by the loading and unloading curves represents the elastically dissipated energy. This energy dissipation is due to the transformation of some of the induced mechanical energy of the applied work to elastic vibrations that are damped by the base material of the repeating units and converted to irreversible thermal energy (heat) with each snap-through buckling event [7,9,17].

The proposed MCCD system avoids a few design disadvantages that limit the practicality of other systems presented in the literature. For example, when multiple units in the MCCD are stacked in parallel (see Sec. 2.2), no design modification is required on the system general configuration nor to the size of the constraining edges (rings) compared with systems comprising curved beams. The reason is that in a loaded MCCD system with units stacked in parallel, each ring is resisting the same horizontal forces while the units in the system are collectively resisting a much larger vertical force than that can be developed by a single unit. Conversely, systems comprising curved beams [10–12] require increasing the size of the constraining edges and hence the horizontal tie to resist the additional forces due to (1) the increased height of the constraining edge and (2) the additional horizontal forces due to each parallelly stacked beam.

Evaluation of curved beams with multiple beams in parallel showed that when the number of beams is increased, the stability state of the whole unit may change from bistable to monostable (for example) due to increased outward lateral deflection of the supporting edges. Thus, a modification to the size of the reaction edges must be made to preserve the required response. A similar examination on the MCCD system showed that the units are independent, in terms of the required constraining for the individual unit, from the overall cumulative vertical force resisted by the system. Thus, there is no need for design adjustments.

Even though it may be argued that this issue can be avoided if a system of curved beams system consisted of many elements in a single layer (horizontal direction), it would still cause a similar

[1]Corresponding author.

Contributed by the Applied Mechanics Division of ASME for publication in the Journal of Applied Mechanics. Manuscript received February 14, 2019; final manuscript received May 16, 2019; published online June 10, 2019. Assoc. Editor: Pedro Reis.

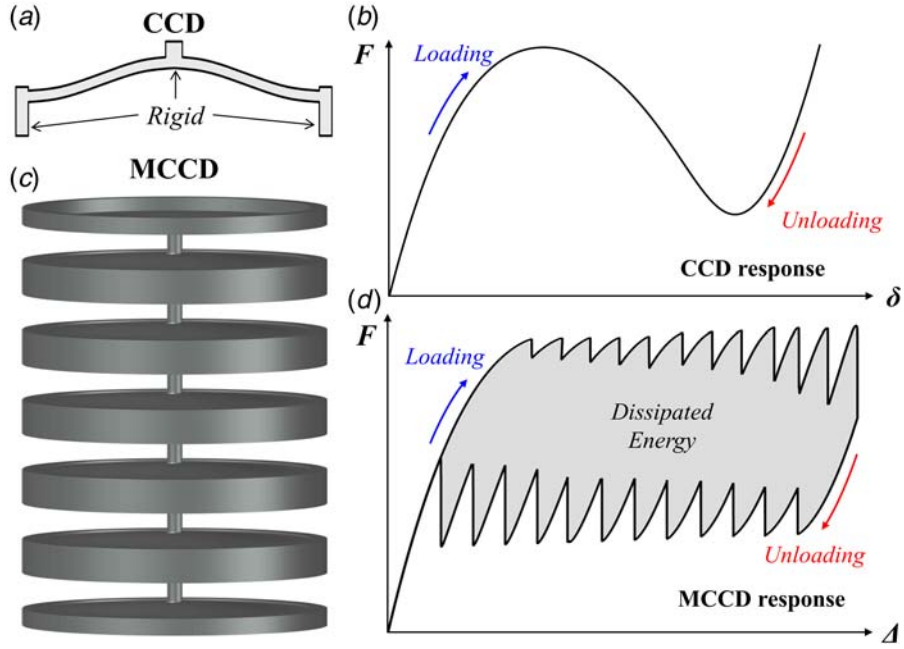

Fig. 1 The MCCD system: (*a*) cross-section of a single CCD unit, (*b*) schematic force–displacement response of a single CCD, (*c*) MCCD composed of multiple CCDs, and (*d*) schematic hysteretic response of an MCCD system. Note that δ is the local CCD displacement, while Δ is the global system displacement.

effect to that discussed above since the horizontal forces will accumulate causing the system to expand in the horizontal direction in an effect analogous to that of Poisson's ratio on a compressed short strut. Thus, the MCCD system avoids this design limitation by having a self-confining feature that makes it a suitable and practical design for civil structural applications where the high force on such systems are expected.

Multilinear models have been presented in the literature to predict the hysteric force–displacement (F–Δ) response of systems with multiple multistable elements [10,18]. These models are more suited for systems comprising units that exhibit a fairly linear force–displacement (F–δ) response. This is because such models do not consider the nonlinear effects on the F–Δ response of the system. For the MCCD system, these nonlinear effects on the F–Δ response are relatively large and this work takes them into account by introducing an effective stiffness concept.

In this work, the behavior of MCCD systems was studied numerically and experimentally. Finite element analyses (FEA) were performed for MCCD systems to study the effects of geometric properties of the dome units (CCDs) on system behavior under displacement controlled loading. A multilinear analytical model that describes the system's F–Δ response is proposed, and the energy dissipation characteristics of the MCCD system are also studied. Finally, experimental tests on 3D printed specimens were conducted to analyze the system and validate numerical results.

2 Multiple Cosine-Curved Dome (MCCD) System

2.1 Response of a Single CCD Unit. The F–δ response of a single CCD incorporates a negative stiffness part that originates from the dome's geometric shape. The cross-sectional profile of the CCD follows the cosine function given in Eq. (1) [19]

$$w(x) = h/2[1 - \cos(2\pi x/l)] \tag{1}$$

where $w(x)$ is the vertical distance at a distance x from the circumference along a horizontal line at the dome's base passing through the center, as shown in Fig. 2. The effective geometric parameters on the response of a CCD are the uniform thickness, t, the base diameter or the span length, l, and the apex height, h, as shown in Fig. 2(*a*). The parameter d is the diameter of the loading area, which has a flat circular shape at the apex region of a CCD. The study in Ref. [16] showed that d has a negligible effect on the response of a CCD if $d/l \leq 0.1$. The circumference edge of a CCD is connected to a rigid ring that constrains edge sliding and rotations under loading, and hence provides fixed boundary conditions for the dome.

The shape of the CCD leads to a highly nonlinear response and a snap-through buckling behavior under a concentrated transverse vertical load at the apex as shown in Fig. 2(*b*). Beyond the buckling point, a CCD deforms to a new configuration, yet the exerted deformations on the CCD are recoverable. For a bistable CCD, an external restoring force is required to recover the original shape, while a monostable CCD is self-recoverable. Figure 3(*a*) shows the typical F–δ responses for monostable and bistable CCDs normalized by their respective buckling load F_b and buckling displacement δ_b. Note that δ denotes the local CCD vertical displacement. It can be seen in Fig. 3(*a*) that the bistable CCD has a negative minimum force F_n at displacement δ_n. In this case, some of the induced energy is trapped in the system and hence the F–δ curve here has a negative force part [4].

The response of a CCD can be divided into three regions [10]: the initial response region (I) with an effective stiffness k_I, the snap-through buckling region (II) with the negative effective stiffness

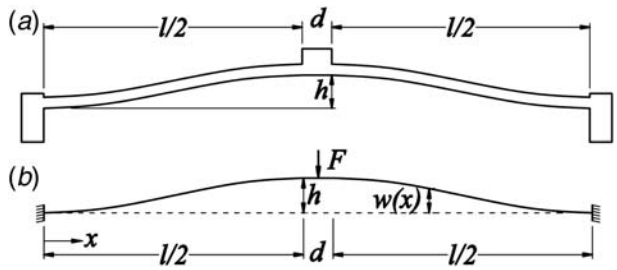

Fig. 2 Geometric parameters of a typical CCD: (*a*) cross-section at the apex and (*b*) idealized system

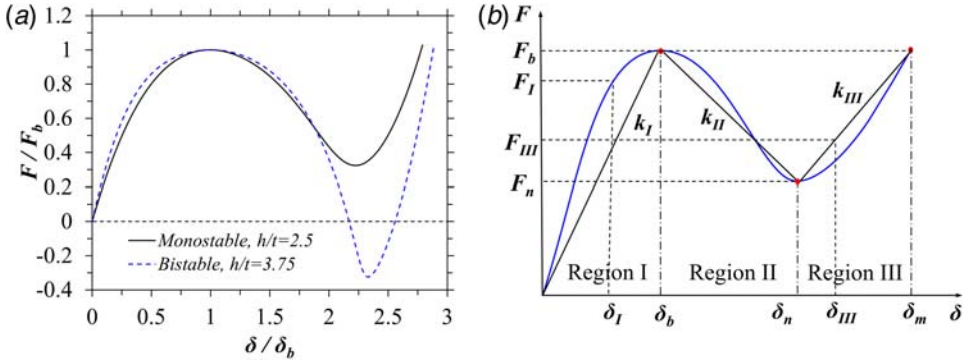

Fig. 3 (*a*) Normalized *F–δ* response for monostable and bistable CCDs and (*b*) multilinear approximation of the *F–δ* response of a CCD

k_{II}, and the post snap-through buckling region (III) with stiffness k_{III}. For given geometric and material properties, the multilinear response of a CCD, as shown in Fig. 3(*b*), can be constructed using the expressions provided in Ref. [16] for F_b, δ_b, F_n, δ_n, and k_{III}. The maximum displacement δ_m is the displacement at a force level equal to F_b in region III, see Fig. 3(*b*); and it can be calculated as $\delta_m = \delta_n + (F_b - F_n)/k_{III}$. Based on these values, the stiffness in each region can be determined. Hence, the linear *F–δ* relations in regions I and III are given as follows:

$$F_I = k_I \delta_I, \quad \delta_I \le \delta_b \tag{2}$$

$$F_{III} = F_n + k_{III}(\delta_{III} - \delta_n) \quad \delta_{III} \ge \delta_n \tag{3}$$

Due to the high nonlinearity of the *F–δ* response of the CCD units, especially in region I, using the above relations (as will be illustrated in Sec. 3) would underestimate and slightly overestimate F_I and F_{III}, respectively, as shown in Fig. 3(*b*). Therefore, the Michaelis–Menten model [20] was used to develop a nonlinear *F–δ* relation for region I. This relation is in terms of *h/t*, δ_b, and F_b and is given in Eq. (4). This model was selected because of its simplicity to determine δ_I for a given force level F_I and because it closely represents the nonlinear path of the *F–δ* response in region I.

$$F_I = \frac{F_b\, A(\delta_I/\delta_b)}{B + (\delta_I/\delta_b)} \tag{4}$$

In Eq. (4), *A* and *B* are constants in terms of *h/t* and can be determined as follows:

$$A = 0.0368(h/t)^3 - 0.3488(h/t)^2 + 0.9559(h/t) + 0.6574$$

and

$$B = 0.0368(h/t)^3 - 0.3488(h/t)^2 + 0.9559(h/t) - 0.3426$$

Similarly, an exponential function was used to develop a relation for the *F–δ* response in region III. The expression is in terms of *h/t*, δ_n, δ_m, F_n, and F_b as given below [21]:

$$F_{III} = F_n + F_b C \left[\frac{\delta_{III}}{\delta_m - \delta_n}\right]^D \tag{5}$$

where *C* and *D* are constants in terms of *h/t* and can be determined by

$$C = -0.0648(h/t)^2 + 0.9261(h/t) - 1.2407$$

and

$$D = 0.0993(h/t)^2 - 0.8157(h/t) + 3.2967$$

2.2 Stacking Configuration of CCD Systems. To have a better understanding on the effect of stacking multiple CCDs on the behavior of the CCD units, a discussion is presented here to analyze the change in *F–Δ* response for different configurations of CCD systems. Note that Δ denotes the global vertical displacement of the MCCD system. There are two basic configurations for stacking CCDs in the vertical direction: parallel and series stacking as shown in Fig. 4, or a combination of the two arrangements. The parallel stacking shown in Fig. 4(*a*) is similar to the case of connected springs in parallel, where the applied load is resisted based on the individual stiffness of each spring but with equal displacement on each one. Denoting the number of stacked CCDs in parallel as n_p, the response of n_p CCDs stacked in parallel (see Fig. 5(*a*)) consists of one buckling event with buckling force $n_p F_b$ at displacement $\Delta_b = \delta_b$, and minimum force $n_p F_n$ at displacement $\Delta_n = \delta_n$. Here, the force is directly scaled by the number of connected CCDs (n_p), assuming that they are identical, while the displacements do not change.

The case of series stacking is similar to the case of connected springs in series, where the load is resisted equally by all springs but with different deformations for each. In this configuration, it is assumed that each CCD is connected to the adjacent CCD by a rigid strut that provides the required height to allow buckling of the unit as shown in Fig. 4(*b*). The rigid rings at the base of each CCD also provide the required height to allow unit buckling.

The response of multiple CCDs stacked in series, where n_s denotes the number of units, is shown in Fig. 5(*b*). The response consists of multiple buckling events with buckling forces of F_b at displacement $\Delta_b = n_s \delta_b$ for the first buckling event. The subsequent minimum force F_n (and its displacement Δ_n) and the next buckling

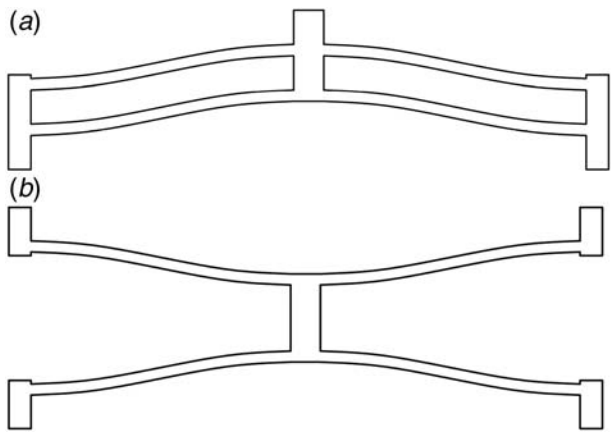

Fig. 4 Possible configurations of CCD units in the vertical direction: (*a*) parallel stacking ($n_p = 2$) and (*b*) series stacking ($n_s = 2$)

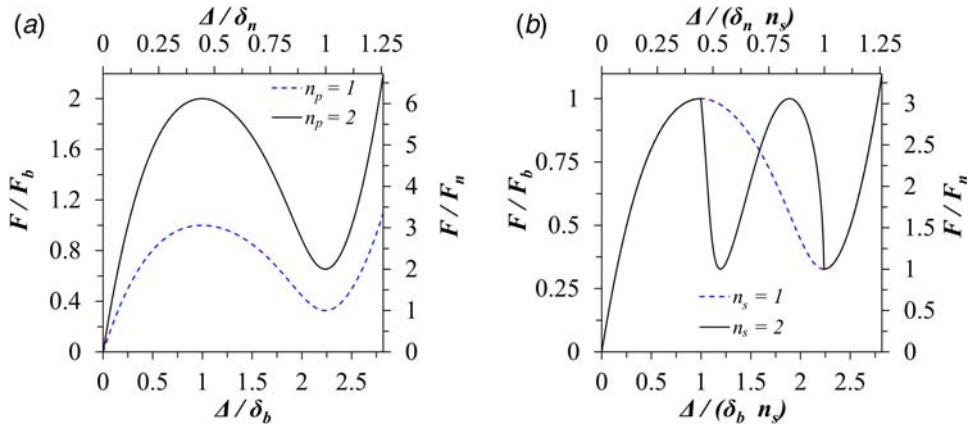

Fig. 5 *F*–Δ curves for CCDs in (*a*) parallel configuration and (*b*) series configuration

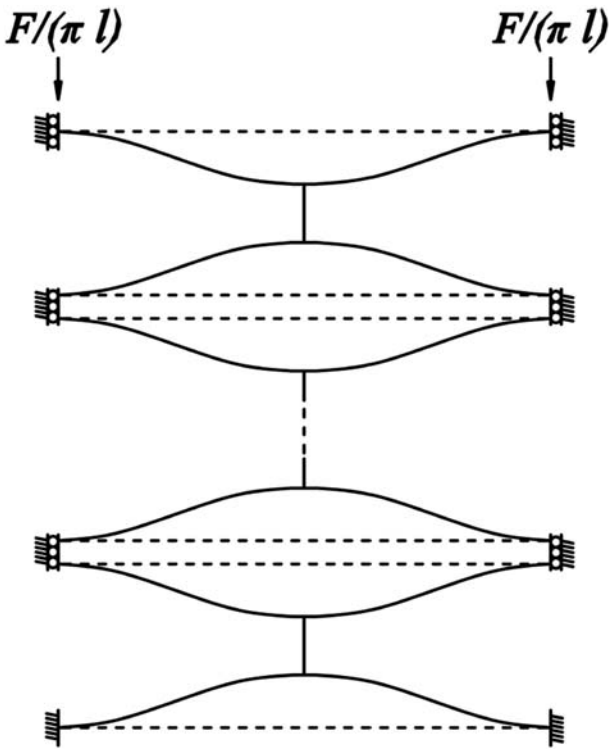

Fig. 6 The idealized MCCD system

displacement depend on the number of CCDs in the system, which is discussed in Sec. 3.

2.3 Finite Element Modeling. Finite element analysis (FEA) was used to examine the *F*–Δ response of the MCCD system. The analyses were performed using the program ABAQUS [22]. The CCD units in the system were modeled as 3D deformable revolved shell objects with four-node shell elements (S4). The material was assumed to have linear elastic isotropic properties. Displacement control was used to apply a dynamic incremental deformation to the system. Large deformations were accounted for by considering the geometric nonlinearity in the analysis. The MCCD system was idealized for the analysis as shown in Fig. 6. The system was analyzed with small variations in the thicknesses of the CCDs to allow a response with consecutive snap-through buckling events.

Figure 7 shows the *F*–Δ response from FEA for two MCCD systems, both with $n_s = 12$. A monostable system (Fig. 7(*a*)) had CCD units with $h = 3$ mm, $l = 140$ mm, and $t = 1.2$, while a bistable system (Fig. 7(*b*)) had $t = 0.8$ mm. The modulus of elasticity E was 1500 MPa, and the Poisson's ratio ν was 0.33.

The type of response (i.e., monostable or bistable) of a CCD unit can be determined by comparing h/t with the critical height-to-thickness ratio $(h/t)_{cr}$ calculated as proposed in Ref. [16]:

$$(h/t)_{cr} = 2.879\,\nu^{-0.052} = 3.05 \tag{6}$$

Thus, the monostable system has CCD units with $h/t = 2.5$, which is smaller than $(h/r)_{cr}$, while the bistable system has CCD units with $h/t = 3.75$, greater than $(h/r)_{cr}$.

A few observations can be made from the *F*–Δ curve in Fig. 7. The force drops after each snap-through and snap-back buckling

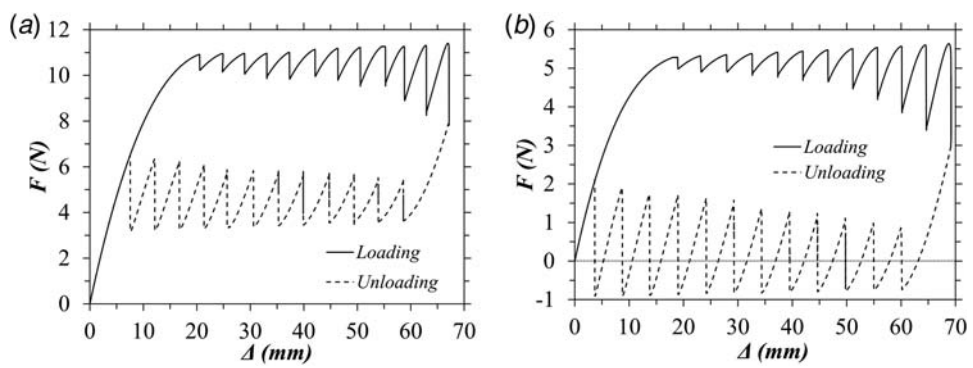

Fig. 7 Force–deformation curves from FEA for MCCD systems: (*a*) monostable and (*b*) bistable

increase in magnitude with every buckling event in the loading and unloading paths. The smallest force drop occurs after the first buckling events, while the largest occurs at the last event. This is also true for the unloading path. The trace of the force–deformation curve between the buckling events has linear and nonlinear segments during the unloading and loading paths, respectively. This is because under loading most of the CCDs in the system are in region I (see Fig. 3(*b*)), which is highly nonlinear, while during unloading most of the CCDs in the system are in region III, which is fairly linear. This also depends on the ratio of k_{III} to k_I, where a higher k_{III}/k_I ratio increases the magnitude of the force drops in the last buckling events during loading and unloading, and vice versa.

3 Analytical Model for MCCD System

This section presents a multilinear model that describes the hysteretic response of the MCCD system. It is assumed that the system consists of similar CCDs stacked in series as shown in Fig. 6. Due to small manufacturing imperfections, each CCD in an MCCD system has a slightly different buckling limit (F_b). This means that each CCD buckles at a different time, which results in a progressive buckling response of the system under displacement control loading. The CCD with lowest buckling force (F_b) buckles first, followed by the one with an immediately higher F_b limit and so forth until buckling of the CCD with the highest F_b in the system is reached. A similar process occurs during unloading, where the unit with highest minimum force (F_n) snaps back first, followed by the one with a lower F_n and so forth until snap-back of the CCD with the lowest F_n in the system.

3.1 Loading Stages. Consider an MCCD system that consists of n_s similar CCD units connected in series, each with an F–δ response as shown in Fig. 3(*b*). Since the system buckles progressively, at any given time, a unit is in one of the regions I, II, and III. Thus, if n_I, n_{II}, and n_{III} denote the number of CCD units in regions I, II, and III [10], respectively, then

$$n_s = n_I + n_{II} + n_{III} \tag{7}$$

To explain the behavior of an MCCD, consider a system composed of four CCDs ($n_s = 4$). Upon applying the force F to the system, the four CCDs resist the same load and their response is within region I ($n_I = 4$). After the first buckling event, three units are still in region I while one CCD is in region II ($n_I = 3$ and $n_{II} = 1$). Since the force drops due to the buckling event, the system relaxes and redistributes the local displacements (δ) of each unit when the buckled CCD reaches region III ($n_I = 3$, $n_{III} = 1$). The same process is repeated until all units are in region III ($n_{III} = 4$). Figure 8 shows the number of CCDs in each region at each loading stage n for a system with $n_s = 4$. From Fig. 8, it can be noted that n_{II} equals to 0 or 1, which means that only one CCD at a time undergoes buckling.

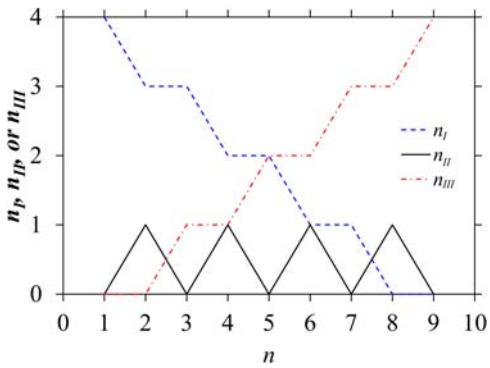

Fig. 8 Number of CCDs in regions I, II, and III during loading stages for a system of $n_s = 4$

The total number of loading stages n_t is related to the number of CCDs connected in series (n_s), as given in Eq. (8) and shown in Fig. 8. The relations between n_I, n_{II}, and n_{III} with n are given in Eqs. (9)–(11). Note that a cosine function is used for n_{II}, which yields 0 for odd n values and 1 for even values

$$n_t = 2n_s + 1 \tag{8}$$

$$n_{II} = |\cos n\pi/2| \tag{9}$$

$$n_I = 0.5[2n_s - n - n_{II} + 1] \tag{10}$$

$$n_{III} = n_s - n_I - n_{II} \tag{11}$$

3.2 Model Development. To develop a multilinear F–Δ response for the MCCD, the hysteretic response was divided into its loading and unloading paths. Each path consists of two groups of points that lie on the actual system F–Δ curve connected by line segments, as shown in Fig. 9(*a*). The first group of points in each path (circles) includes the points at the force level F_b with displacement spacing s_b for the loading path, and the points with a force level of F_n and displacement spacing s_n in the unloading path. The second group of points in each path (squares) includes the buckling drop forces F_{bd} (from F_b) at counterpart displacements for the loading path, and the minimum drop force F_{nd} (from F_n) at counterpart displacements for the unloading path. Figure 9(*a*) shows a schematic F–Δ response for the MCCD system with the quantities used to develop the multilinear model. The figure also shows the actual and the multilinear F–Δ curves during loading and unloading.

3.2.1 Loading Path. The unknowns in the first group of points (at F_b level) are the system displacements at each of the snap-through bucking events Δ_{bi}. The displacement at the first buckling event (Δ_{b0}), for $i = 0$, is determined based on the well-known equivalent spring concept [23] for n_s springs connected in series with similar stiffness k_I and resisting the same force F_b. The equivalent stiffens of such a system is k_I/n_s, and hence $\Delta_{b0} = F_b/(k_I/n_s) = n_s\,\delta_b$.

FEA results, as those in Fig. 7, show that the spacing between the snap-through buckling events is constant. After the system experiences a local CCD snap-through, it reloads (when the buckled CCD reaches region III) and it encounters another local snap-through event when the load reaches F_b. The spacing s_b is constant and a property of the individual CCD unit F–δ responses. As shown in Fig. 9(*b*), this constant spacing (s_b) is the distance between δ_b and δ_m and hence $s_b = \delta_m - \delta_b$. Thus, s_b represents the required displacement for the MCCD system to reload and reach F_b after snap-through buckling of a CCD unit. Thus, the points defining the local CCD buckling events in the system loading path, i.e., the system displacements (Δ_{bi}) and the corresponding system buckling forces (F_{bi}), can be determined as follows:

$$\Delta_{bi} = n_s\delta_b + is_b \tag{12}$$

$$F_{bi} = F_b \tag{13}$$

where i is the buckling event (see Fig. 9(*a*)) and $i = 0, 1, 2, \ldots, (n_s - 1)$.

When the system approaches F_b during loading, CCDs in regions I and III approach δ_b and δ_m, respectively. When the system reaches F_b, a given CCD snaps-through and the force level drops until the buckled CCD in region II reaches δ_n. Deformations for the CCDs are then redistributed at the system displacement Δ_{bi}, leading to CCDs in regions I and III to a reduced force level F_{bdi}. This means that during the load drop, the response of one CCD unit transitions from region I to III. Otherwise, if the buckled CCD were to

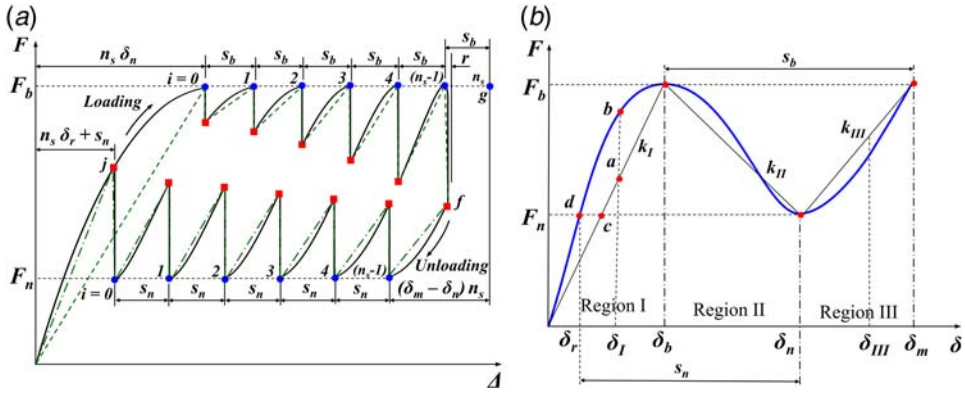

Fig. 9 (*a*) Schematic *F*–Δ response of the MCCD system with quantities used to develop the multilinear model and (*b*) actual and multilinear *F*–*δ* responses of a CCD unit

remain at δ_n the value of F_{bdi} would equal F_n, which is not the case. Consequently, the local displacements δ_I and δ_{III} shown in Fig. 9(*b*) for a CCD in regions I and III decrease below δ_b and δ_m, respectively. Mathematically this is expressed as

$$\delta_I < \delta_b \tag{14}$$

$$\delta_{III} = \delta_n + \delta_{III}{}' < \delta_m \tag{15}$$

where $\delta_{III}{}'$ is the local displacement component in region III.

Since the system is connected in series, all CCDs are experiencing the same force F_{bdi}. Thus, by determining either δ_I or $\delta_{III}{}'$, the force F_{bdi} can be calculated using Eqs. (2) or (3), respectively. Based on the concept of connected springs in series, the contribution of CCDs in regions I and III toward the system response Δ_{bi} is given by

$$(n_s - i - 1)\delta_I + (i+1)\delta_{III} = \Delta_{bi} \tag{16}$$

A linear relation between δ_I and $\delta_{III}{}'$ using the stiffnesses k_I and k_{III}, respectively, can be established based on the concept of two springs connected in series and resisting an equal load. This relation is given by $\delta_I\, k_I = \delta_{III}\, k_{III}$ and hence

$$\delta_{III}{}' = \delta_I k_I / k_{III} \tag{17}$$

By substituting Eqs. (15) and (17) into Eq. (16), the local displacement for CCDs in region I during the force drop, δ_{Ibdi}, and hence F_{bdi} can be calculated as follows:

$$\delta_{Ibdi} = \frac{\Delta_{bi} - (i+1)\ \delta n}{(n_s - i - 1) + (i+1)\ \dfrac{k_I}{k_{III}}} \tag{18}$$

$$F_{bdi} = \delta_{Ibdi} k_I \tag{19}$$

Due to the nonlinear response of the CCD units during the loading branch, the approach followed to develop Eq. (17), i.e., assuming that the two springs are linear, underestimates F_{bdi}. This can be corrected by replacing k_I in Eq. (18) by the effective stiffness for the CCD units in region I, k_{eI}, which mainly depends on n_s. The value of k_{eI} can be calculated at the last point in the loading curve, namely, point *f*, as shown in Fig. 9(*a*). This point was chosen to determine k_{eI} because it reduces the unknowns in Eq. (16) to one. The displacement at this point (Δ_{bf}) with $i = n_s - 1$ is slightly greater than that determined by Eq. (12) since it is associated with the last buckling event of the system. The additional distance *r* (see Fig. 9(*a*)) and hence Δ_{bf} can be determined with

$$r = (\delta_n - \delta_b)/n_s \tag{20}$$

and

$$\Delta_{bf} = n_s \delta_b + (n_s - 1)s_b + r \tag{21}$$

Thus, at $i = n_s - 1$, Eq. (16) reduces to $n_s\, \delta_{III} = \Delta_{bf}$ and hence δ_{III} can be determined. The local displacement for CCDs in region III at point *f* (i.e., δ_{IIIf}) and the drop force (F_{bdf}) are determined as

$$\delta_{IIIf} = \Delta_{bf}/n_s \tag{22}$$

$$F_{bdf} = F_n + (\delta_{IIIf} - \delta_n)k_{III} \tag{23}$$

Now the equivalent local displacement δ_{If} for CCDs in region I for a force equal to F_{bdf} can be determined by

$$\delta_{If} = F_{bdf}/k_I \tag{24}$$

By using Eq. (17) for $i = n_s - 1$ and $\delta_{Ibdi} = \delta_{If}$, k_{eI} can be calculated as follows:

$$k_{eI} = \frac{(\Delta_{bf} - n_s\ \delta_n)\ k_{III}}{n_s\ \delta_{If}} \tag{25}$$

The modified expression for δ_{Ibdi} with k_I replaced by k_{eI} in Eq. (18) is given in Eq. (26). The force drop for the loading path can now be determined as given earlier in Eq. (19)

$$\delta_{Ibdi} = \frac{\Delta_{bi} - (i+1)\ \delta n}{(n_s - i - 1) + (i+1)\ \dfrac{k_{eI}}{k_{III}}} \tag{26}$$

Figure 10(*a*) shows the *F*–Δ response of an MCCD system with eight monostable CCDs as obtained from FEA and the analytical model relations just presented above. Visual comparison of the responses shows that the analytical F_{bdi} values are almost equal to each other and generally smaller (larger force drops) than those from the FEA, which is a consequence of using linear equations to determine k_{eI} and F_{bdi}.

As can be seen in Fig. 9(*b*) for points *a* and *b*, Eq. (19) will underestimate F_{bdi} because of the nonlinearity of the CCD units' *F*–*δ* response. Therefore, the simulated response can be improved by using the nonlinear expression for F_I in Eq. (4) to determine k_{eI} and F_{bdi} for the loading path, which is shown in Fig. 10(*b*).

3.2.2 Unloading Path. Similar to the approach followed for the loading path, the unknowns in the first group of points (at F_n level) are the system displacements at each snap-back event Δ_{ni}. The displacement at the first snap-back event (at $i = n_s - 1$) is determined in the analogous form to the way in which Δ_{b0} was determined for the loading path but with point *g* as the origin (see Fig. 9(*a*)). The displacement at point *g* can be determined using Eq. (12) for Δ_{bi} with $i = n_s$. Before the first snap-back event, all CCDs are in region III with k_{III}. Consequently, the equivalent system stiffness

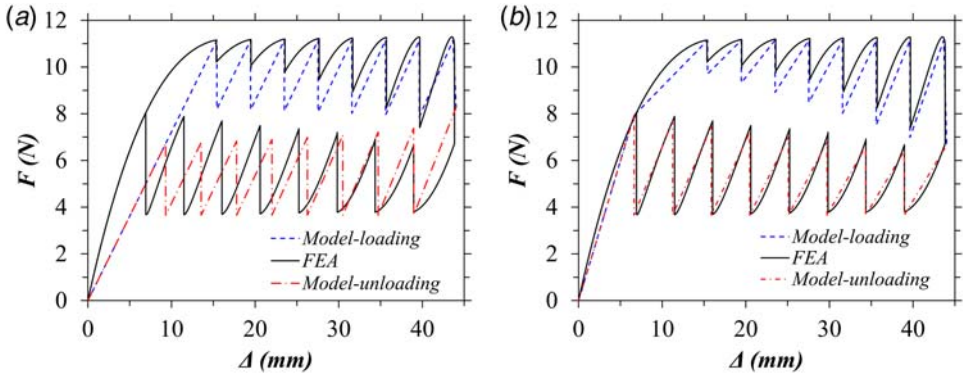

Fig. 10 ***F*–Δ curves from FEA and analytical model using (*a*) linear equations and (*b*) nonlinear equations to calculate k_{el}, k_{elll}, F_{bdi}, and F_{ndi}**

is k_{III}/n_s and the displacement from point g is $n_s(\delta_m - \delta_n)$, as shown in Fig. 9(*a*).

The spacing s_n in the unloading path was also found to be constant and a property of the F–δ response of each CCD unit. The spacing s_n is the distance required to reach the snap-back critical point, which is the distance between δ_n and δ_r, or $s_n = \delta_n - \delta_r$ as shown in Fig. 9(*b*). It should be noted that determining δ_r linearly with stiffness k_I (i.e., using Eq. (2)) results in some error that underestimates s_n. Thus, δ_r can be determined from Eq. (4) by equating F_I to F_n and solving for δ_I. Points c and d in Fig. 9(*b*) show the effect of using linear and nonlinear relations for region I to determine δ_r.

The system displacements during unloading (Δ_{ni}) and the corresponding snap-back forces F_{ni} can be determined as follows:

$$\Delta_{ni} = n_s\delta_r + (i+1)s_n \tag{27}$$

$$F_{ni} = F_n \tag{28}$$

A similar procedure to that was followed to determine F_{bdi} for the loading path is followed to determine the force drops for the unloading path F_{ndi}. The contribution of CCDs in regions I and III toward the system response Δ_{ni} at each snap-back event is given by

$$(n_s - i)\delta_I + i\delta_{III} = \Delta_{ni} \tag{29}$$

Thus, the local displacement component ($\delta_{III'ndi}$) for CDDs in region III at the force drop can be determined by Eq. (30), where k_{eIII} is the effective stiffness for units in region III. Hence, the force F_{ndi} can be calculated using Eq. (3) or Eq. (5).

$$\delta_{III'bdi} = \frac{\Delta_{ni} - i\,\delta_n}{(n_s - i)\,\dfrac{k_{eIII}}{k_I} + i} \tag{30}$$

The stiffness k_{eIII} can be calculated at the last point in the unloading curve j, see Fig. 9(*a*). The displacement at point j (Δ_{nj}) is $n_s\,\delta_r + s_n$. At point j, with $i = 0$, Eq. (29) reduces to $n_s\,\delta_I = \Delta_{nj}$. Thus, the local displacement at point j (δ_{Ij}) for CCDs in region I is given by

$$\delta_{Ij} = \Delta_{nj}/n_s \tag{31}$$

By using δ_{Ij} in Eq. (2), or in Eq. (4) for more accurate results, F_{ndj} can be calculated. This is followed by calculating the local displacement component at point j ($\delta_{III'j}$) for CCDs in region III using Eq. (3) or Eq. (5) for $F_{III} = F_{ndj}$. By using Eq. (30) with $i = 0$ and $\delta_{III'j}$, k_{eIII} can be found as follows:

$$k_{eIII} = \frac{\Delta_{nj}\,k_I}{n_s\,\delta_{III'j}} \tag{32}$$

Figure 10 shows the simulated unloading path using linear (Fig. 10(*a*)) and nonlinear (Fig. 10(*b*)) equations to determine k_{eIII} and F_{ndi}, plotted along FEA results. It can be seen that using linear relations underestimates s_n and F_{ndi} values.

4 Experimental Validation

The MCCD specimen shown in Fig. 11 was fabricated using a 3D polymer-based printer (Stratasys Fortus 250 mc) with acrylonitrile butadiene styrene (ABS) filament. The ABS material had a Poisson's ratio of 0.35; and the compressive modulus of elasticity of the 3D printed CCDs, determined according to ASTM D695, had an average value of 853 MPa.

The printed MCCD system consisted of 10 CCDs with average "as-printed" dimensions of $t = 0.75 \pm 0.03$ mm, $h = 1.76 \pm 0.03$ mm, $l = 50 \pm 1$ mm, and $d = 4.5$ mm. The units in the system were designed to ensure that the maximum resisted vertical force (F_b) by a CCD unit at the critical section, which is the loading region at the apex, to be much lower than the force that would cause a punching shear failure. This can be typically achieved by increasing t or d (with $d/l \leq 0.1$). The specimens were 3D printed monolithically with oversized confining rings. The thickness of the rings was 4.5 mm. Generally, for a CCD specimen, a ring thickness that ranges from 4 to 8 times t was found to be sufficient to eliminate the influence of rotational stiffness and lateral expansion on the behavior of the element. Visual examination of the edges did not show signs of rotation along the edge during load application, or after load removal (damage).

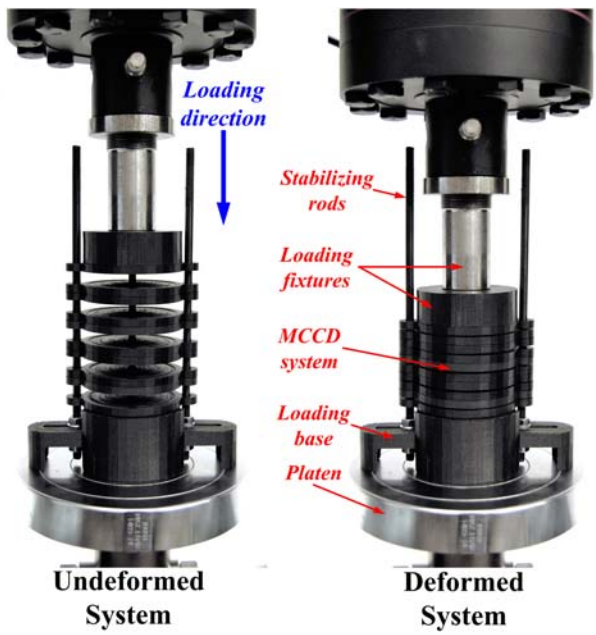

Fig. 11 Test setup for an MCCD system with ten CCDs ($n_s = 10$)

The test was performed using a universal testing machine with a custom fixture (indenter) to apply a vertical load on the rigid ring of the top CCD as shown in Fig. 11. Testing was conducted under displacement control, applying an incremental displacement at a rate of 0.1 mm/s.

To stabilize the MCCD system against side sway that may occur during testing, the CCD units were designed and 3D printed with two collars on each side as shown in Fig. 11. This allowed the CCDs to slide in the vertical direction between two rods that were inserted into the collars. The two rods were fixed to a loading base (see Fig. 11), and the distance between them could be adjusted via slots in the loading base. The rods were fixed to the base using nuts and washers on each side. During testing, the guiding rods were coated with a lubricant to minimize friction between them and the collars in the CCD units. This issue can be avoided in MCCD systems that are composed of more than one chain (i.e., one column) of CCD units.

Figure 12 shows the experimental F–Δ response of the MCCD specimen compared with the simulated response using the model presented in Sec. 3. The experimental response shows that the buckling force at each buckling event gradually increased. This is because the dimensions of the printed CCD units slightly vary and hence F–δ response of each CCD is different. This does not only vary the buckling force levels but also the corresponding displacements at the buckling events.

Since the F–δ response for each CCD varies, each unit has a different k_I. Thus, the initial effective stiffness of the manufactured MCCD system is higher than that of the simulated response based on the average dimensions. This effect triggers the first buckling event on the weakest CCD in the system earlier than the calculated average buckling displacement $\Delta_{b0} = n_s \delta_b$. This is because the effective stiffness of the MCCD system is greater than the calculated average stiffness based on average dimensions ($F_b/n_s \delta_b$). Therefore, during loading, the CCD in the system with the lowest F_b reaches its buckling point (δ_b, F_b), while other CCDs in the system are below their buckling limit. Although the buckling limit variation among CCD units complicates calculating an accurate response for the system, it is an essential feature to obtain a progressive buckling response and hence elastic energy dissipation.

In spite of the complications noted above, it can be noted in Fig. 12 that the simulated F–Δ curve agrees fairly well with the experimental response. This is largely due to the fact that the displacements of the CCD units in the system are minimally affected by dimension variations.

To study the effect of loading rate on the response of the MCCD system, the test was repeated for loading rates of 1, 3, 9, and 15 mm/s. The resulting F–Δ curves are shown in Fig. 13. The figure shows that the loading rate had a minimal effect on the response of the system over the examined range of 0.1–15 mm/s. However, it can be noted that with increased loading rate, the force drops in the loading and unloading paths decrease slightly. The locations of snap-through and snap-back events also slightly change due to the loading rate. Studies [13,24] on the dynamic behavior of discrete chains with multistable elements indicate that the loading rate (in addition to other factors) has dynamic effects on the response of such systems. In fact, even at quasistatic loading conditions, discrete systems exhibit high-frequency vibrations upon snap-through events [24]. These damped vibrations are the main contributors to the dissipated energy by discrete systems even at very low loading rates.

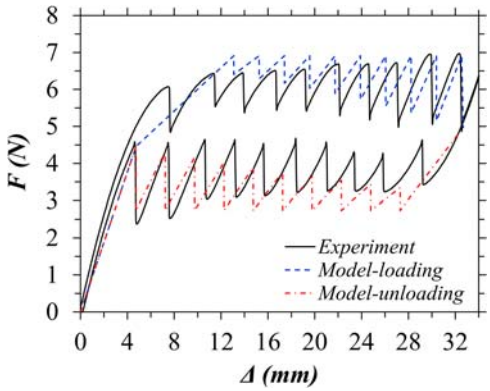

Fig. 12 F–Δ curves for MCCD system from experimental tests and the analytical model

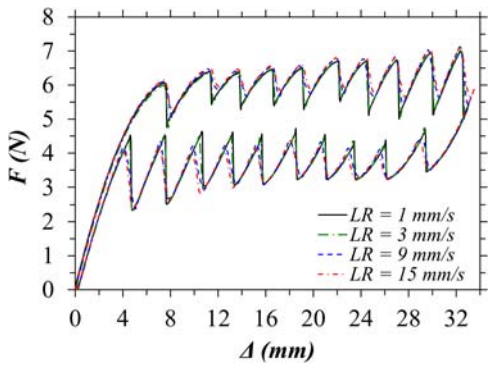

Fig. 13 Experimental F–Δ curves for an MCCD system at varying loading rates: 1, 3, 9, and 15 mm/s

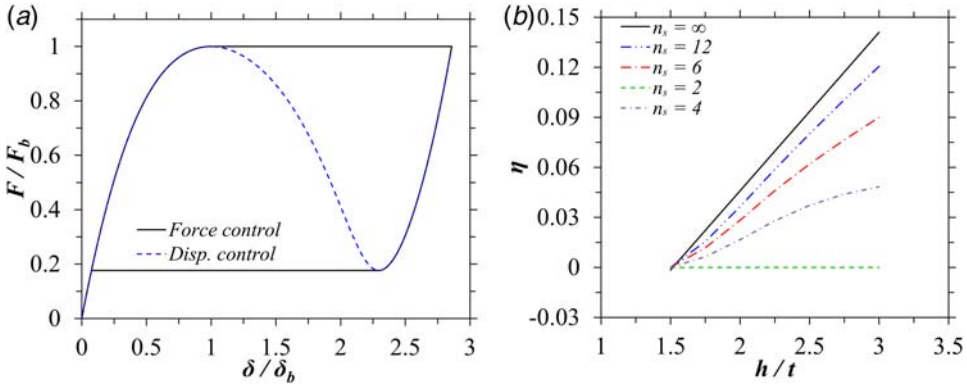

Fig. 14 (*a*) Normalized F–δ curve for a CCD with $h/t = 2.75$ under force and displacement control conditions and (*b*) loss factor with h/t for different n_s values

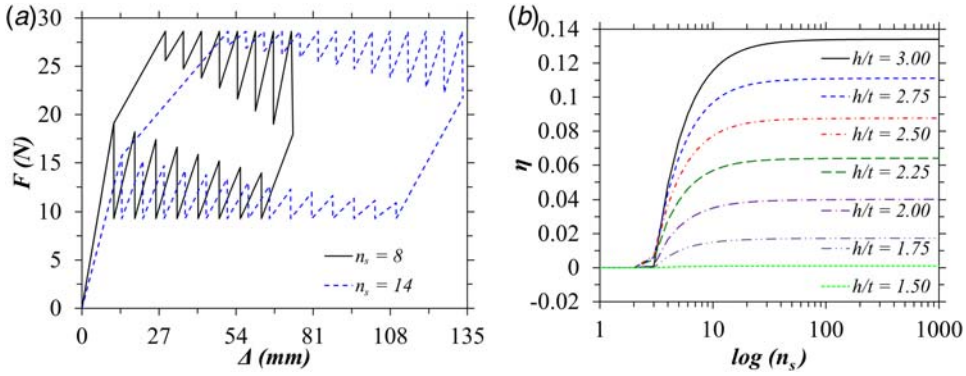

Fig. 15 (*a*) F–Δ curves for MCCDs with $h/t = 2.5$ and $n_s = 8$ and 14 and (*b*) loss factor with n_s for different h/t ratios

5 Energy Dissipation Characteristics

The dissipated energy by the MCCD system can be quantified by a general measure of damping called the loss factor η [25]. This factor is defined as the ratio of the dissipated energy U_d to the total applied work to deform the system W in one loading/unloading cycle as given in Eq. (33). W is the area under the F–Δ curve from zero displacement to the maximum displacement at point f in Fig. 9(*a*), while U_d is the enclosed area by the F–Δ curve

$$\eta = U_d/(2\pi W) \tag{33}$$

The main parameters of the MCCD system that affect η are h/t and n_s. The effect of h/t can be studied by knowing the maximum value of η. The theoretical maximum value of η for an MCCD system with n_s CCDs of a specific h/t occurs when $n_s \to \infty$. The F–Δ response of such a system is similar to the F–δ response of a single CCD under force control conditions. Figure 14(*a*) shows the F–δ response of a monostable CCD with $h/t = 2.75$ under force and displacement control conditions, where the area enclosed by the force control curve represents the specific maximum dissipated energy. This condition was used to construct a relation between η and h/t, which was found to be linear, as shown in Fig. 14(*b*).

The other main parameter of the MCCD system that affects η is n_s. The analytical multilinear model presented in Sec. 3 was used to calculate η by varying n_s for a range of h/t values. Figure 15(*a*) shows the F–Δ response of two MCCD systems with $t = 2$ mm, $h = 5$ mm, $l = 200$ mm, and $n_s = 8$ and 14. The curves show that increasing n_s highly decreases the magnitude of the force drops from F_b and F_n with each snap-through and snap-back event, thus increasing the dissipated energy.

To examine the relation between η and n_s the developed model was used to determine η for $n_s = 1$ to 1000 and for h/t values ranging from 1.5 to 3 as shown in Fig. 15(*b*). The study in Ref. [16] showed that a CCD requires h/t of about 1.5 to exhibit a snap-through instability and h/t of about 3 to change the stability state from monostable to bistable, where self-recoverability (preferred) does not occur. From Fig. 15(*b*), it can be noted that for $n_s \le 2$, $\eta = 0$, which means that the loading and unloading paths coincide. For an MCCD system with $2 < n_s \le 12$, η increases sharply with n_s over this range, indicating hysteretic responses. For $n_s > 12$, a plateau is reached and a further increase in n_s results in very small increases (<10%) in η. The same finding can be deduced from the curves in Fig. 14(*b*). The n_s–η relation in Fig. 15(*b*) shows that 90% of the maximum value of η is reached with $n_s = 12$.

6 Conclusions

A new system able to dissipate energy through elastic instabilities was presented. The MCCD system proposed in this paper comprises multiple cosine-curved domes that exhibit elastic snap-through buckling behavior, which permits the system to display hysteretic force–deformation response and thus capable of elastically dissipating energy. Numerical studies and experimental tests were conducted to determine the most effective parameters of system response and energy dissipation characteristics. An analytical multilinear model that describes the hysteretic force–displacement response was proposed. The model takes into account the nonlinear effects of the building units of the MCCD system and was shown to yield accurate simulations. The following findings of the MCCD system were drawn:

(1) The proposed MCCD system can dissipate strain energy by the creation of a hysteretic response through the successive elastic snap-through and snap-back responses of cosine-curved domes connected in series. The hysteretic response is elastic, thus featuring fully recoverable deformations, and has low rate dependence.
(2) The amount of dissipated energy mainly depends on the number (n_s) and the height-to-thickness ratio (h/t) of the building units (CCDs). The relation between η and h/t is linear while the relation between η and n_s is nonlinear. Nonetheless, the higher n_s and h/t are the higher the amount of the dissipated energy.
(3) The proposed MCCD system showed a maximum loss factor (η) value of about 0.14 for a monostable (self-recoverable) system and even higher for a bistable system.
(4) The loss factor reaches about 90% of its theoretical maximum value for MCCD systems with about 12 CCDs ($n_s = 12$). A further increase in n_s yields a very small increase in the value of η.
(5) Although increasing n_s increases the amount of dissipated energy, it also decreases the initial stiffness of the MCCD system. This can be compensated by increasing the number of CCDs linked in parallel and/or using more chains of CCDs.

References

[1] Hu, N., and Burgueño, R., 2015, "Buckling-Induced Smart Applications: Recent Advances and Trends," Smart Mater. Struct., **24**(6), pp. 1–20.
[2] Puglisi, G., and Truskinovsky, L., 2002, "Rate Independent Hysteresis in a Bi-Stable Chain," J. Mech. Phys. Solids, **50**(2), pp. 165–187.
[3] Bažant, Z. P., and Cedolin, L., 2010, *Stability of Structures: Elastic, Inelastic, Fracture and Damage Theories*, World Scientific, Singapore.
[4] Shan, S., Kang, S. H., Raney, J. R., Wang, P., Fang, L., Candido, F., Lewis, J. A., and Bertoldi, K., 2015, "Multistable Architected Materials for Trapping Elastic Strain Energy," Adv. Mater., **27**(29), pp. 4296–4301.
[5] Ha, C. S., Lakes, R. S., and Plesha, M. E., 2018, "Design, Fabrication, and Analysis of Lattice Exhibiting Energy Absorption via Snap-Through Behavior," Mater. Des., **141**, pp. 426–437.
[6] Chen, T., Mueller, J., and Shea, K., 2016, "Design and Fabrication of a Bistable Unit Actuator With Multi-Material Additive Manufacturing," Annu. Int. Solid Free. Fabr. Symp., pp. 2060–2076.

[7] Liu, S., Imaniazad, A., and Burgueño, R., 2019, "Architected Materials for Tailorable Shear Behavior With Energy Dissipation," Extrem. Mech. Lett., **28**, pp. 1–7.
[8] Frenzel, T., Findeisen, C., Kadic, M., Gumbsch, P., and Wegener, M., 2016, "Tailored Buckling Microlattices as Reusable Light-Weight Shock Absorbers," Adv. Mater., **28**(28), pp. 5865–5870.
[9] Findeisen, C., Hohe, J., Kadic, M., and Gumbsch, P., 2017, "Characteristics of Mechanical Metamaterials Based on Buckling Elements," J. Mech. Phys. Solids, **102**, pp. 151–164.
[10] Restrepo, D., Mankame, N. D., and Zavattieri, P. D., 2015, "Phase Transforming Cellular Materials," Extrem. Mech. Lett., **4**, pp. 52–60.
[11] Correa, D. M., Klatt, T., Cortes, S., Haberman, M., Kovar, D., and Seepersad, C., 2015, "Negative Stiffness Honeycombs for Recoverable Shock Isolation," Rapid Prototyp. J., **21**(2), pp. 193–200.
[12] Rafsanjani, A., Akbarzadeh, A., and Pasini, D., 2015, "Snapping Mechanical Metamaterials Under Tension," Adv. Mater., **27**(39), pp. 5931–5935.
[13] Liu, J., Qin, H., and Liu, Y., 2018, "Dynamic Behaviors of Phase Transforming Cellular Structures," Compos. Struct., **184**, pp. 536–544.
[14] Haghpanah, B., Shirazi, A., Salari-Sharif, L., Guell Izard, A., and Valdevit, L., 2017, "Elastic Architected Materials With Extreme Damping Capacity," Extrem. Mech. Lett., **17**, pp. 56–61.
[15] Kidambi, N., Harne, R. L., and Wang, K. W., 2017, "Energy Capture and Storage in Asymmetrically Multistable Modular Structures Inspired by Skeletal Muscle," Smart Mater. Struct., **26**(8), pp. 1–15.
[16] Alturki, M., and Burgueño, R., 2019, "Response Characterization of Multistable Shallow Domes With Cosine-Curved Profile," Thin Wall. Struct., **140**, pp. 74–94.
[17] Chen, Q., Zhang, X., and Zhu, B., 2018, "Design of Buckling-Induced Mechanical Metamaterials for Energy Absorption Using Topology Optimization," Struct. Multidiscip. Optim., **58**(4), pp. 1395–1410.
[18] Benichou, I., and Givli, S., 2013, "Structures Undergoing Discrete Phase Transformation," J. Mech. Phys. Solids, **61**(1), pp. 94–113.
[19] Vangbo, M., 1998, "An Analytical Analysis of a Compressed Bistable Buckled Beam," Sens. Actuators A Phys., **69**(3), pp. 212–216.
[20] Raaijmakers, J. G. W., 1987, "Statistical Analysis of the Michaelis-Menten Equation," Biometrics, **43**(4), pp. 793–803.
[21] Pardo, S. A., 2016, *Empirical Modeling and Data Analysis for Engineers and Applied Scientists*, Springer, NJ.
[22] Dassault Systèmes, 2012, "Abaqus User Manual." Abaqus Standard Version, Providence, RI.
[23] Radomirovic, D., and Kovacic, I., 2015, "An Equivalent Spring for Nonlinear Springs in Series," Eur. J. Phys., **36**(5), pp. 1–6.
[24] Feeny, B. F., and Diaz, A. R., 2010, "Twinkling Phenomena in Snap-Through Oscillators," J. Vib. Acoust., **132**(6), pp. 1–19.
[25] Carfagni, M., Lenzi, E., and Pierini, M., 1998, "The Loss Factor as a Measure of Mechanical Damping," Proceedings of the 16th International Modal Analysis Conference, Santa Barbara, CA, Feb. 2–5, **3243**, pp. 580–584.